JCTC Journal of Chemical Theory and Computation

Article

pubs.acs.org/JCTC

The Development of a Classical Force Field To Determine the Selectivity of an Aqueous Fe^{3+}–EDA Complex for TcO_4^- and SO_4^{2-}

Christopher D. Williams,[†,‡] Neil A. Burton,*[,‡] Karl P. Travis,[†] and John H. Harding[†]

[†]Department of Materials Science and Engineering, University of Sheffield, Sheffield, S1 3JD, U.K.

[‡]School of Chemistry, University of Manchester, Manchester, M13 9PL, U.K.

Supporting Information

ABSTRACT: A classical force field has been developed in order to investigate the selective exchange of oxyanions (TcO_4^- vs SO_4^{2-}) with other ligands (H_2O, Cl^-) to an aqueous Fe^{3+}–ethylenediamine (EDA) complex. Potentials of mean force for a range of exchange reactions were generated using umbrella sampling and classical molecular dynamics simulations in order to calculate the affinity of each oxyanion for the Fe^{3+}–EDA complex in aqueous solution. In order to accurately introduce a degree of specificity for the interaction of Fe^{3+} with each ligand type, force field parameters were tuned to match the results of density functional theory calculations. Preferential exchange of H_2O, Cl^-, and SO_4^{2-} for TcO_4^- via an interchange mechanism is observed, in agreement with experimental observations. Both the relative solvation entropies and enthalpies of the anions were found to be critically important factors governing the magnitude of the observed selectivities. These results have important implications for the design and modeling of functionalized materials for the remediation of land contaminated with radioactive ^{99}Tc.

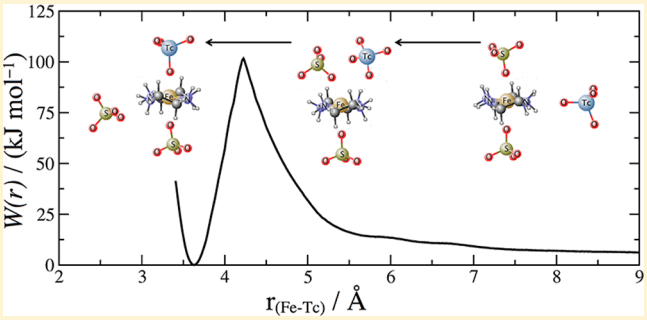

INTRODUCTION

The radioactive fission product ^{99}Tc is discharged from nuclear reprocessing operations, such as the PUREX process at Sellafield.[1] Because of its long half-life (2.1×10^5 years), the presence of Tc poses a significant problem to the environmental remediation of contaminated sites resulting from the nuclear legacy.[2] The difficulty with removal of Tc from discharge plumes or groundwater stems from its anionic nature in solution; Tc forms a tetrahedral pertechnetate oxyanion (TcO_4^-), which enhances its mobility in the environment, resulting in a tendency to accumulate in crustaceans, enter the food chain, and contribute to the total radioactive dose to humans.[3] Additionally, competing oxyanions similar in shape and size to TcO_4^-, such as sulfate (SO_4^{2-}), are present in vast excess in the environment. Any method proposed for the cleanup of TcO_4^- must, therefore, be highly selective. Many of the current options for TcO_4^- remediation reduce Tc to its insoluble +4 oxidation state and so are heavily reliant on specific reducing conditions.[4] These methods may also suffer from poor selectivity in the presence of competing anions. One possible solution to the ^{99}Tc cleanup problem is the use of a family of novel sorbent materials known as self-assembled monolayers on mesoporous supports (SAMMS).[5] SAMMS consist of a physically robust mesoporous amorphous silica support, typically MCM-41, which has a tunable and uniform pore size ranging from 15 to 100 Å.[6,7] The mesopores are modified with functional monolayers to target specific atoms, molecules, or ions, making SAMMS highly selective and an attractive prospect for environmental remediation problems.[8]

Fryxell et al. developed a SAMMS material in which three ethylenediamine (EDA) functionalities, tethered to the surface of MCM-41 by short alkyl chains, coordinate a Cu^{2+} ion, forming an octahedral complex.[9] These workers then performed adsorption experiments to study the selectivity of this Cu^{2+}–EDA monolayer toward oxyanions. The material was found to be highly selective for CrO_4^{2-} and $H_2AsO_4^-$, demonstrating almost complete removal of these contaminant species even in the presence of high concentrations of the competing SO_4^{2-}. They proposed a mechanism, confirmed by EXAFS experiments,[10] in which the oxyanion binds directly and monodentately to Cu^{2+} by ligand exchange, displacing the amine termini on two of the tethered EDA ligands. The adsorption of other oxyanions, such as MoO_4^{2-}, SeO_4^{2-}, and PO_4^{3-}, to this material has also been investigated.[11,12] Yoshitake et al. studied the adsorption of $H_2AsO_4^-$ to MCM-41 functionalized with various transition-metal EDA complexes.[13] These workers proposed the formation of an octahedral transition-metal complex with two bidentate EDA ligands and two Cl^- ligands (present due to the use of $FeCl_3$ in the synthetic procedure), although it was not suggested whether the Cl^- ions were *cis* or *trans* to each other. It is also possible that H_2O ligands occupy a small number of these coordination

Received: March 7, 2014
Published: June 24, 2014

sites. They observed that the Fe^{3+}−EDA complex had a far greater oxyanion capacity than Cu^{2+} and showed that adsorption to the complex was largely unaffected by competing SO_4^{2-} and Cl^- ions. Mattigod and co-workers[14] investigated a related functionalized material in which a Cu^{2+}−EDA complex was tethered by short alkyl chains to the surface of TiO_2 nanoparticles and used it to achieve the selective removal of TcO_4^- from groundwater containing competing anions, including SO_4^{2-}, and obtained distribution coefficients as high as 4000 mL/g. This process, in which TcO_4^- displaces a H_2O ligand, demonstrates the ability of these transition-metal complexes to bind a monoanion, TcO_4^-, in preference to a dianion, SO_4^{2-}. There is uncertainty over the exact mechanism of oxyanion adsorption to these functionalized materials, and an explanation for the observed selectivity is required. If the argument were based purely on electrostatic attraction between Fe^{3+} and the oxyanion, SO_4^{2-} would be expected to have a greater affinity for the complex than TcO_4^-, in conflict with the experimental observations.

Computer simulations can be used to complement experiment and give a molecular level insight into the oxyanion exchange process, allowing future optimization of the structure of the material and maximizing the selectivity toward the oxyanion species of interest. In this work, we have simulated the selective adsorption of oxyanions, specifically, TcO_4^- and SO_4^{2-}, to Fe^{3+}−EDA complexes in aqueous solution via a ligand exchange mechanism (shown in Figure 1), analogous to

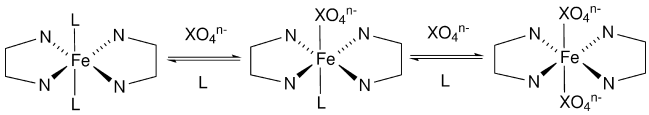

Figure 1. Exchange of ligands, L (L = Cl^-/H_2O), with a general oxyanion, XO_4^{n-} (X = Tc/S), to the Fe^{3+}−EDA complex studied in this work. EDA hydrogen atoms are omitted for clarity, and each species is in aqueous solution.

that proposed experimentally in ref 13. For our purposes, it is assumed that the observed selectivity is dependent only on the chemistry of the Fe^{3+}−EDA complex, so neither the alkyl tethers nor the inorganic support were considered.

The ligand exchange process is considered within the context of the thermodynamic cycle in Figure 2, where the overall Gibbs free energy change, $\Delta G_{ex,aq}$, is defined as the difference in free energy when the oxyanion is in solution compared to when it is coordinated to the complex. $\Delta G_{ex,aq}$ can be expressed in terms of the free energy of gas phase exchange, $\Delta G_{ex,g}$, and the reactant and product solvation free energies, $\Delta G_{solv,R}$ and $\Delta G_{solv,P}$, respectively. The most common computational approach to determine $\Delta G_{ex,aq}$ is to perform quantum mechanical calculations combined with a suitable continuum model for the surrounding solvent. This method can be used to compute ΔG_{solv} for neutral molecules reasonably accurately; however, the assumptions that the electrostatic interactions between a solute and the solvent are independent of the solvent's explicit molecular structure and that the dielectric response of the medium is uniform are poor for ionic species, leading to errors commonly exceeding 20 kJ mol^{-1} even for singly charged ions. In our case, some of the ions have a higher charge, leading to larger errors, and since the determination of $\Delta G_{ex,aq}$ requires the combination of several of these calculations, this approach was deemed too inaccurate and unreliable in preliminary studies. Conversely, an approach involving atomistic simulations using a more general transferable force field was also found to not be able to account fully for the electronic subtleties of the d-block coordination complexes or ligand polarizabilities. Here, ligand specific parameters will be developed to address these limitations.

The first step outlined in this paper is to compare the stabilities of the *cis* and *trans* isomers of the Fe^{3+}−EDA complex using density functional theory (DFT). The optimized structures are then used to parametrize a force field that describes the specific interaction of each ligand with the Fe^{3+}−EDA complex. Using this force field, molecular dynamics (MD) simulations were performed in conjunction with an umbrella sampling technique to determine a potential of mean force (PMF) for the exchange of TcO_4^- and SO_4^{2-} with other ligands on the Fe^{3+}−EDA complex. For each ligand exchange process, $\Delta G_{ex,aq}$ was directly obtained from the PMF, allowing a comparison of the relative affinities of TcO_4^- and SO_4^{2-}. We then calculated the enthalpic, $\Delta H_{ex,aq}$, and entropic, $T\Delta S_{ex,aq}$, contributions to ligand exchange in order to explain the observed selectivity. Finally, the implications of our findings for the use of oxyanion-SAMMS as a TcO_4^- remediation option are discussed.

COMPUTATIONAL DETAILS

Development of a Classical Force Field. Gas phase geometry optimizations of the Fe^{3+}−EDA complex and oxyanions were performed with DFT using the hybrid meta M06 exchange correlation functional, which is known to perform reasonably well for transition metals.[15] All atoms were represented using the 6-311+G(d,p) basis set, apart from Tc, which was described using the def2-TZVP basis set[16,17] and the 28-electron effective core potential.[16] The relative stabilities of the two isomers of the solvated Fe^{3+}−EDA complexes were compared by computing their energies at the optimized geometry using the CPCM implicit solvation model. All quantum mechanical calculations were carried out using Gaussian 09.[18]

The basic functional form of the force field includes harmonic bond stretch and angle bend terms

$$V(r) = k_r(r_{ij} - r_{eq})^2 \quad (1)$$

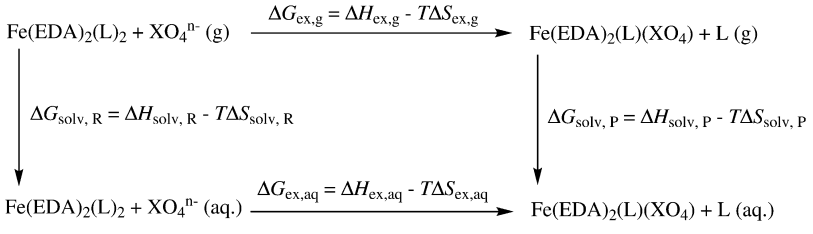

Figure 2. Contributions to the aqueous ligand exchange process. L = H_2O/Cl^- and X = Tc/S.

dx.doi.org/10.1021/ct500198c | J. Chem. Theory Comput. 2014, 10, 3345−3353

$$V(\theta) = k_\theta(\theta_{ijk} - \theta_{eq})^2 \quad (2)$$

where k_r and k_θ are the force constants for bond stretching and angle bending, respectively, with the corresponding equilibrium values of r_{eq} and θ_{eq}. A triple cosine potential was used for dihedral angles

$$V(\varphi) = \sum_{n=1}^{n=3} A_n[1 + (-1)^{n-1}\cos(n\varphi_{ijkl})] \quad (3)$$

where A_1, A_2, and A_3 are the Fourier coefficients. Nonbonded interactions were evaluated as the sum of van der Waals (VDW), represented using a Lennard-Jones 12-6 potential, and Coulomb terms

$$V(r) = \frac{q_1 q_2}{4\pi\varepsilon_0 r_{ij}} + 4\varepsilon_{ij}\left[\left(\frac{\sigma_{ij}}{r_{ij}}\right)^{12} + \left(\frac{\sigma_{ij}}{r_{ij}}\right)^{6}\right] \quad (4)$$

where q_i is the partial atomic charge of atom i and ε_0 is the vacuum permittivity. The cross-interaction parameters ε_{ij} and σ_{ij} were determined using the Lorentz−Berthelot combining rules.[19] Nonbonded interactions were calculated for both intermolecular atom pairs and intramolecular pairs separated by more than two bonds.

For the oxyanions, equilibrium bond lengths and angles were set to the quantum mechanically optimized values and force constants for SO_4^{2-} were taken from the literature.[20] Classical force field parameters for TcO_4^- have not previously been reported in the literature, so the corresponding force constants for this oxyanion were obtained by fitting to a potential energy surface generated at the DFT level. These force constants were determined by calculating the second derivative of the variation in potential energy by finite difference about the Tc−O bond or O−Tc−O angle. Initial partial charges were determined quantum mechanically by fitting to an electrostatic potential according to the Merz−Singh−Kollmann scheme,[21,22] and for short-range interactions, OPLS parameters were used[23] apart from σ_{Tc} and ε_{Tc}, which were taken from Cundari et al.[24] For the Fe^{3+}−EDA complex, all bonds were constrained using the SHAKE algorithm[25] and angle bend parameters from the AMBER force field[26] were used. For the EDA ligands, both the van der Waals and the torsional parameters were taken from the OPLS force field.[23,27] Additional N−Fe−N harmonic angle potentials were employed to maintain either *cis* or *trans* geometry about the Fe^{3+} cation, necessary due to the inability of a classical force field of this type to maintain this feature of the geometry of the transition-metal complex. Water was represented using the extended simple-point charge (SPC/E) model,[28] and the Cl^- ion parameters used are known to accurately reproduce experimental solvation free energies.[29]

To simulate the ligand exchange process, the force field must be able simultaneously to reproduce the behavior of each anion in solution as well as in the coordination environment of the highly polarizing Fe^{3+} cation. To achieve this, nonbonded parameters were optimized to match the gas phase potential energy of each interaction, shown in Figure 3, at the DFT level between each species to within 1 kJ mol^{-1} and 0.05 Å, respectively. The conjugate gradient method, implemented using DL_POLY Classic,[30] was used for this fitting procedure. First, nonbonded parameters (σ_O, ε_O, and q_O) were adjusted to fit the interaction of each oxyanion with water. Second, the van der Waals diameter for Fe^{3+}, σ_{Fe}, was adjusted to have a different value for each individual ligand interaction (TcO_4^-, SO_4^{2-}, Cl^-, and H_2O); this is necessary to account for the large variations in polarization of the ligands by Fe^{3+}. The full set of force field parameters used in this study is given in the Supporting Information.

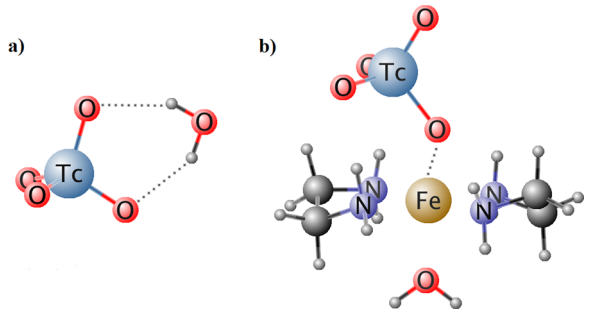

Figure 3. Models used to parametrize the classical force field by fitting to the energy and equilibrium bond distances of the DFT interaction of TcO_4^- with (a) water and (b) *trans* Fe^{3+}−EDA. An analogous fitting procedure was used for SO_4^{2-}.

Molecular Dynamics Simulations. MD simulations were used to study the structure of solvated oxyanions, XO_4^{n-}, and the Fe^{3+}−EDA complex as well as to determine potentials of mean force (PMFs) corresponding to each ligand exchange event. In every case, the oxyanions and Fe^{3+}−EDA complexes were solvated by the random addition of approximately 1100 H_2O molecules in a cubic box of dimension 32 Å, followed by equilibration for 0.1 ns before generating statistics. DL_POLY Classic[30] was used to conduct the simulations in which the equations of motion were integrated using the Verlet leapfrog algorithm.[19] Cubic periodic boundary conditions were used to account for the effects of bulk solution, and long-range electrostatic interactions were evaluated using the Ewald summation method.[19] van der Waals forces were spherically truncated at 10 Å, and a 2 fs time step was used. Simulations were conducted in the NPT ensemble at 298 K and 1 atm, maintained using the Nosé−Hoover thermostat and barostat[31,32] with relaxation times of 0.1 ps. The structure and coordination environment of both the oxyanions and the Fe^{3+}−EDA complexes were estimated from the radial distribution function (RDF) for the distance between Fe^{3+} and the ligand obtained during a 10 ns simulation.

Potential of Mean Force Simulations for Oxyanion Exchange. We require a PMF that describes the relative change in free energy between the situation where the anion is coordinated to Fe^{3+}−EDA and the situation when it is completely solvated (at large separation from the Fe^{3+}−EDA) and another ligand occupies this coordination site. The PMF for exchange of Cl^- with a H_2O of $[Fe(EDA)_2(H_2O)_2]^{3+}$ was first calculated for comparison with the oxyanions and elucidate the likely initial complex. PMFs were then obtained for each oxyanion ligand exchanging with a H_2O of $[Fe(EDA)_2(H_2O)_2]^{3+}$ and with a Cl^- of $[Fe(EDA)_2(Cl)_2]^+$ to study their relative $\Delta G_{ex,aq}$ for the possible initial complexes as well as a PMF for the direct exchange of TcO_4^- with a SO_4^{2-} of $[Fe(EDA)_2(SO_4)_2]^-$, in the case where the complex has previously become saturated with an excess of SO_4^{2-}.

Free energy processes with large barriers cannot be obtained from a conventional MD simulation. In this work, we have used the umbrella sampling method[33] to explore unfavorable regions of phase space. The method works by adding a biasing potential, enabling the entire path along the relevant reaction coordinate to be sufficiently sampled. The biasing potential was

dx.doi.org/10.1021/ct500198c | J. Chem. Theory Comput. 2014, 10, 3345−3353

applied using the PLUMED plugin,[34] and the reaction coordinate for oxyanion exchange was defined as the distance between Fe^{3+} and the central atom of the oxyanion, X. We have used a biasing potential that takes the same form as eq 1, where the target distance between Fe and X, r_{eq}, was gradually decreased in 0.25 Å intervals in adjacent simulation "windows" from 10 to 3 Å. The force constant of the biasing potential, k_r, was typically set to 200 kJ mol^{-1} $Å^{-2}$. Each simulation lasted for 2 ns, the final 1 ns of which was used for the collection of statistics used to generate the PMFs. The overall potential energy function was then corrected for the bias and recombined to give the PMF, $W(r)$, using the equation

$$W(r) = -RT \ln P(r) \quad (5)$$

and the weighted histogram analysis method (WHAM).[35] The WHAM approach calculates the unbiased probability of the reaction coordinate, $P(r)$, by separating the distributions of r into a series of bins along the reaction coordinate and determining a relative free energy difference between each bin. During the equilibration period, WHAM was also used to check for sufficient statistical overlap between sampling in adjacent windows along the reaction coordinate. If there was insufficient overlap (i.e., in the region where the PMF profile is steep), additional simulations with larger biasing force constants were conducted. $\Delta G_{ex,aq}$ is directly obtainable from the PMF by taking the difference in free energy at the minimum energy point, r_{min}, and at the maximum separation of 10 Å. Since the simulations were conducted in the NPT ensemble, the enthalpy associated with each exchange event, $\Delta H_{ex,aq}$, was computed over the same interval by taking the difference in mean ensemble enthalpy from extended simulations restrained at r_{min} and 10 Å lasting 10 ns. $\Delta H_{ex,aq}$ was also calculated for each of the *cis* isomers of the complex. Finally, the entropic contribution to exchange, $T\Delta S_{ex,aq}$, was computed by subtracting the difference in enthalpy, $\Delta H_{ex,aq}$, from $\Delta G_{ex,aq}$.

RESULTS

Structure of Solvated Oxyanions. The calculation of $\Delta G_{ex,aq}$ associated with any oxyanion ligand exchange event involves computation of ΔG_{solv}, which is strongly dependent on the specific interactions of each oxyanion with the solvent. The DFT optimized structure of TcO_4^- using the M06 functional is tetrahedral and predicts a Tc−O bond length of 1.705 Å, in better agreement with the experimental value (1.724 Å)[36] than a previously published theoretical bond length of 1.756 Å[37] that employed the B3LYP functional and the Los Alamos effective core potential with its associated double-ζ basis set for Tc.[38] The SO_4^{2-} oxyanion has a shorter calculated bond length of 1.487 Å, so it will require a much smaller cavity in solution than TcO_4^-, suggesting that less free energy is required to form the solvent cavity. The final force field parameters for each oxyanion, fitted using the DFT structures, are given in Table 1. There is no literature data to compare with our TcO_4^- force field parameters, but the optimized SO_4^{2-} parameters are very similar to other classical force fields,[39] giving us confidence in our parametrization approach.

The oxyanion RDFs, $g(r)$, are compared in Figure 4 to show the differences in structure of the surrounding water molecules. In the notation used, $g_{i-OW}(r)$ refers to the RDF between anion atom i and oxygen in water. The TcO_4^- $g_{X-OW}(r)$ and $g_{O-OW}(r)$ peaks associated with the first and second solvation shells are much less intense than those for SO_4^{2-}, due to the higher charge of SO_4^{2-}. The primary $g_{X-OW}(r)$ peak for TcO_4^- is also at a much greater radial distance (4.30 Å) than the corresponding SO_4^{2-} peak (3.79 Å), mainly due to the difference in size between the two oxyanions but also, in part, due to the larger TcO_4^- oxygen van der Waals diameter, σ_O. A shelflike feature that appears in the second solvation shell in $g_{O-OW}(r)$ near 5.5 Å (X = Tc) and 5.0 Å (X = S) is due to the interaction of waters held in the first solvation shell with O atoms on the opposite side of the oxyanion. This was also observed in a previously obtained RDF for SO_4^{2-} in water[39] and appears to be characteristic of oxyanions in aqueous solution. The solvent structure is representative of bulk solution beyond approximately 8 Å. The appearance of peaks and troughs in each RDF up to this distance is indicative of long-range order in the solvent, suggesting that the solvation of oxyanions is associated with a negative $T\Delta S_{solv}$ term. The implication of the more ordered structure associated with SO_4^{2-} solvation is that $T\Delta S_{solv}$ is expected to be more unfavorable than for TcO_4^-. Despite the bare SO_4^{2-} ion being smaller than TcO_4^- the integral of $g_{X-OW}(r)$ was calculated to determine that, for SO_4^{2-}, there are more water molecules in its primary solvation shell (13−14) than for TcO_4^- (11−12).

Potential of Mean Force for Water Exchange on Fe^{3+}−EDA. The optimized Fe van der Waals diameters, σ_{Fe}, for each ligand type are given in Table 2. A simulation of the *trans* isomer of the Fe^{3+}−EDA complex in solution was performed to investigate its coordination environment. The RDF between

Table 1. Final Optimized Force Field Parameters Used for the TcO_4^- and SO_4^{2-} Oxyanions

nonbonded				
i		q_i (e)	ε_i (kJ mol^{-1})	σ_i (Å)
TcO_4^-	Tc	+2.720	1.0080	2.655
	O	−0.930	0.2090	3.860
SO_4^{2-}	S	+2.300	0.8370	3.550
	O	−1.075	0.6500	3.250
bond stretch				
i−j		k_r (kJ mol^{-1} $Å^{-2}$)		r_{eq} (Å)
Tc−O		2094.5		1.7045
S−O		2198.7		1.4870
angle bend				
i−j−k		k_θ (kJ mol^{-1} rad^{-2})		θ_{eq} (deg)
O−X−O		585.8		109.47

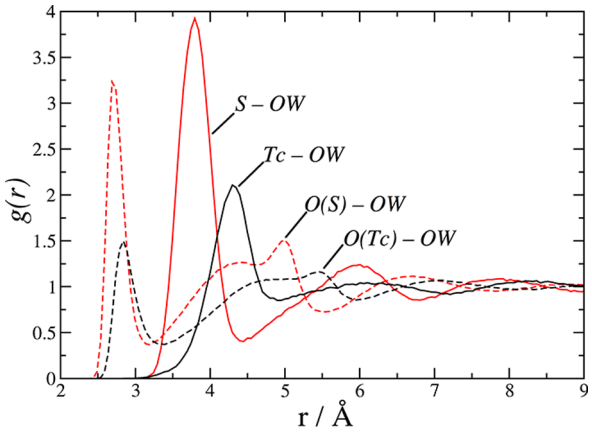

Figure 4. RDFs for XO_4^{n-} in solution. $g_{X-OW}(r)$ is represented by solid lines and $g_{O-OW}(r)$ by dashed lines. X = Tc (black) and X = S (red).

dx.doi.org/10.1021/ct500198c | J. Chem. Theory Comput. 2014, 10, 3345−3353

Table 2. Final Optimized Fe^{3+} VDW Diameters, σ_{Fe}, for Each Ligand Interaction

ligand	σ_{Fe} (Å)
H_2O (O)	1.465
TcO_4^- (O)	2.600
SO_4^{2-} (O)	1.820
Cl^-	3.095
other atom types	1.700

Fe^{3+} and OW (Figure 5), $g_{Fe-OW}(r)$, has an intense peak at 2.4 Å, associated with water molecules directly coordinated to the

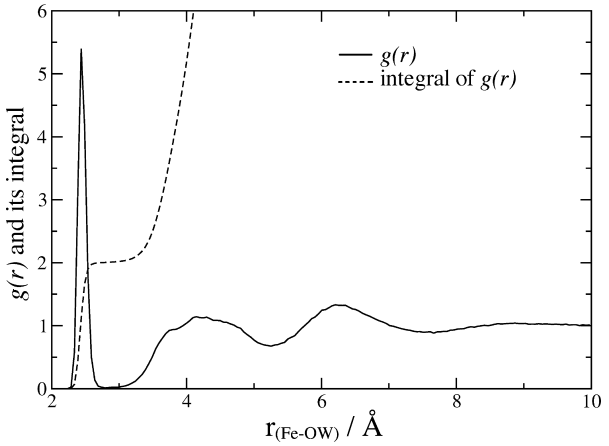

Figure 5. RDF (solid line) and its integral (dashed line) between Fe^{3+} and OW, obtained from a simulation of the Fe^{3+}–EDA complex in water.

complex, and the integral of $g_{Fe-OW}(r)$ clearly shows that this peak is associated with two H_2O ligands, which occupy the axial positions in this case.

Providing that a ligand exchange event has a free energy barrier, $\Delta G_{barrier}$, low enough for it to occur several times during a typical MD simulation, the RDF can be used to estimate the PMF, $W(r)$, using the equation

$$W(r) = -RT \ln g(r) \quad (6)$$

where R is the universal gas constant and T is the simulation temperature. During the simulation, a number of H_2O exchange events take place, enabling the PMF to be either estimated by using the RDF and eq 6 or obtained using the umbrella sampling approach (eq 5). The barriers to exchange for these two approaches (Figure 6) are 15.1 and 14.9 kJ mol^{-1}, respectively, where the difference can be explained by the limited statistical sampling of the higher energy region in the former approach. Although the shapes of the two PMFs are similar, the one obtained from this first approach does not tend to zero, suggesting that one H_2O ligand is favored over all others. This discrepancy can be rationalized by the fact that the RDF method accounts for both possible axial ligand sites, whereas the umbrella sampling method gives the free energy change associated with a single H_2O ligand exchange. The 14.9 kJ mol^{-1} barrier obtained by umbrella sampling, which corresponds to a H_2O exchange rate of 15.2 ns^{-1}, is much smaller than the experimentally determined barrier for a fully solvated Fe^{3+} ion[40] (60.4 kJ mol^{-1}) and is evidence of the H_2O labilizing effect of the chelating EDA ligands.

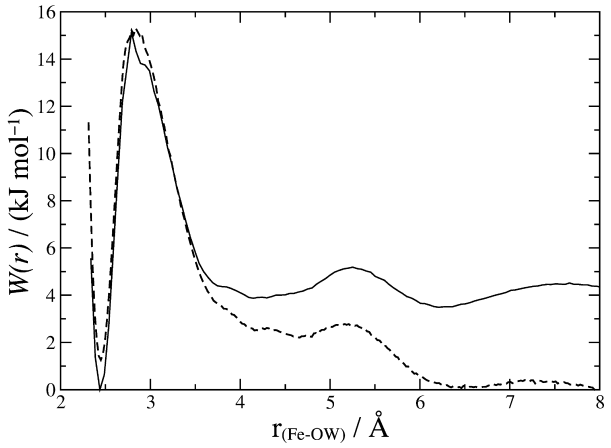

Figure 6. PMFs for H_2O exchange at the axial positions of the Fe^{3+}–EDA complex, estimated from the RDF (solid line), eq 6, and obtained from umbrella sampling simulations and eq 5 (dashed line).

PMF for Anion Exchange with Water on Fe^{3+}–EDA. The aqueous free energy for ligand exchange, $\Delta G_{ex,aq}$, is directly obtainable from the PMF profiles, and for each process, the enthalpic, $\Delta H_{ex,aq}$, and entropic, $T\Delta S_{ex,aq}$, contributions to $\Delta G_{ex,aq}$ (at 298 K) are summarized in Table 3, as well as the free energy required to overcome the barrier to exchange, $\Delta G_{barrier}$.

Experimentally, a Fe^{3+} complex will be tethered to a mesoporous support through the addition of ferric chloride salt to the uncomplexed EDA-functionalized pore. $\Delta G_{ex,aq}$ for Cl^- exchange with H_2O was found to be −127.1 kJ mol^{-1} with a favorable $T\Delta S_{ex,aq}$ term (+22.9 kJ mol^{-1}), so the initial solvated (tethered) complex is certain to be coordinated by Cl^-, in agreement with the experimental EXAFS observations.[13] Since the DFT results predict the *trans* isomer of this complex to be more stable than *cis* by 19.6 kJ mol^{-1}, it is reasonable to assume the *trans*-$[Fe(EDA)_2(Cl)_2]^+$ complex to be thermodynamically favored. DFT calculations also show that the *cis* isomer of $[Fe(EDA)_2(H_2O)_2]^{3+}$ is lower in energy than its *trans* counterpart by 7.2 kJ mol^{-1}; however, for the sake of comparison with experimental observations of anion exchange, and given that this aqua complex is only likely to be present in very low concentrations, all of the PMFs generated in this work correspond to the *trans* Fe^{3+}–EDA complex.

Figure 7 shows that the exchange of either oxyanion for H_2O has a significant free energy driving force; $\Delta G_{ex,aq}$ is −165.4 and −160.5 kJ mol^{-1} for TcO_4^- and SO_4^{2-}, respectively, with the minimum energy in distance at 3.62 and 3.65 Å. For TcO_4^- exchange, $\Delta H_{ex,aq}$ is favorable (−190.2 kJ mol^{-1}) but $T\Delta S_{ex,aq}$ is unfavorable (−24.8 kJ mol^{-1}). $\Delta H_{ex,aq}$ for SO_4^{2-} exchange is less favorable (−131.1 kJ mol^{-1}) but does have a favorable $T\Delta S_{ex,aq}$ term (+29.4 kJ mol^{-1}). Both oxyanions were found to coordinate to the Fe^{3+}–EDA complex in a monodentate fashion, in agreement with the experimental observation in ref 13. The exchange of these ligands for H_2O is primarily driven by electrostatic attraction between the anion and Fe^{3+}. However, entropy also plays an important role in the selectivity of Fe^{3+}–EDA for oxyanions; the effect of SO_4^{2-} inducing greater long-range order in the surrounding H_2O molecules than TcO_4^- means that removing it from its fully solvated environment and coordinating to the Fe^{3+}–EDA complex is more favorable entropically. TcO_4^- is, therefore, vastly preferred to SO_4^{2-} in terms of enthalpy, but the overall

dx.doi.org/10.1021/ct500198c | J. Chem. Theory Comput. 2014, 10, 3345−3353

Table 3. Contributions to $\Delta G_{ex,aq}$ at 298 K for Each Ligand Exchange Event on the *trans* Fe^{3+}–EDA Complex (kJ mol^{-1})

initial complex	final complex	$\Delta G_{ex,aq}$	$\Delta H_{ex,aq}$	$T\Delta S_{ex,aq}$	$\Delta G_{barrier}$
$[Fe(EDA)_2(H_2O)_2]^{3+}$	$[Fe(EDA)_2(H_2O)(TcO_4)]^{2+}$	−165.4	−190.2	−24.8	12.6
$[Fe(EDA)_2(H_2O)_2]^{3+}$	$[Fe(EDA)_2(H_2O)(SO_4)]^{+}$	−160.5	−131.1	29.4	0.0
$[Fe(EDA)_2(H_2O)_2]^{3+}$	$[Fe(EDA)_2(H_2O)(Cl)]^{2+}$	−127.1	−104.2	22.9	15.9
$[Fe(EDA)_2(Cl)_2]^{+}$	$[Fe(EDA)_2(Cl)(TcO_4)]^{+}$	−26.4	−74.5	−48.1	66.7
$[Fe(EDA)_2(Cl)_2]^{+}$	$[Fe(EDA)_2(Cl)(SO_4)]^{0}$	−60.0	−54.6	5.4	30.3
$[Fe(EDA)_2(SO_4)_2]^{-}$	$[Fe(EDA)_2(SO_4)(TcO_4)]^{0}$	−4.6	−36.9	−32.3	97.0

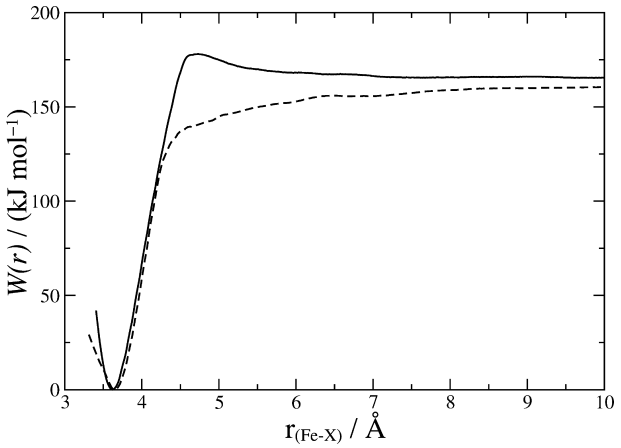

Figure 7. PMFs for XO_4^{n-} exchange with H_2O. X = Tc (solid line) and X = S (dashed line).

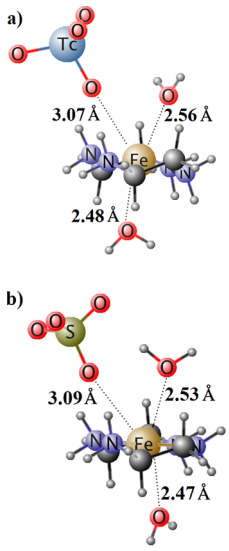

Figure 8. Snapshots of typical configurations at the point of XO_4^{n-} exchange with H_2O showing average Fe^{3+}–ligand distances: (a) X = Tc, from the 4.75 Å window, (b) X = S, from the 4.5 Å window.

calculated $\Delta G_{ex,aq}$ shows that SO_4^{2-} competes for Fe^{3+}–EDA, suggesting that the relative solvation entropies of the oxyanions, $T\Delta S_{solv}$, are a critically important property for exchange reactions of this type. There is an apparent discrepancy in that it might be expected that $T\Delta S_{ex,aq}$ associated with transferring Cl^- from solution to the complex (+22.9 kJ mol^{-1}) would be similar to the equivalent TcO_4^- process (−24.8 kJ mol^{-1}) as their identical overall charge will lead to them having a similar $T\Delta S_{solv}$. This apparent discrepancy can be explained by considering that Cl^- is almost completely removed from its solvation environment on coordination to the complex, whereas TcO_4^- still has three oxygens that are still solvated. For TcO_4^- exchanging with H_2O, $\Delta H_{ex,aq}$ was the same for the *cis* complex (−190.1 kJ mol^{-1}) as the *trans* isomer. For SO_4^{2-}, exchange was less favorable (−119.6 kJ mol^{-1}) by 11.5 kJ mol^{-1} compared to the equivalent process on the *trans* complex.

The difference in the shapes of the PMF profiles suggests that exchange with H_2O occurs by a slightly different mechanism for the two oxyanions; there is a small free energy barrier for TcO_4^- exchange but not for SO_4^{2-}. Significant free energy barriers were not observed along this reaction coordinate, suggesting that the exchange of oxyanions with H_2O is not a kinetically limited process. Oxyanion exchange occurs at approximately 4.7 Å for TcO_4^- and 4.5 Å for SO_4^{2-}, respectively. Typical atomic configurations from the simulation windows corresponding to these distances are compared in Figure 8. Despite the difference in the shape of the PMF profiles, at the point of exchange, the average Fe^{3+}–O (XO_4^{n-}) and Fe^{3+}–OW distances are similar. Analysis of the PMF profile shows that the coordination number of the complex is always 6 during the exchange of either oxyanion, and since no significant low energy intermediate complexes are observed, this suggests that oxyanion exchange occurs via an interchange mechanism in both cases.

PMF for Oxyanion Exchange with Chloride on Fe^{3+}–EDA. $\Delta G_{ex,aq}$ for the exchange of oxyanions with Cl^- is obtained from the PMF profile in Figure 9, giving −26.4 kJ mol^{-1} for TcO_4^- and −60.0 kJ mol^{-1} for SO_4^{2-}, suggesting that this complex is selective for SO_4^{2-} by 33.6 kJ mol^{-1}. The reason for the selectivity difference is due to the more repulsive short-range interaction with Cl^- stemming from the larger σ_O parameter for TcO_4^-. These processes require free energy to overcome barriers of 66.7 and 30.3 kJ mol^{-1}, for TcO_4^- and

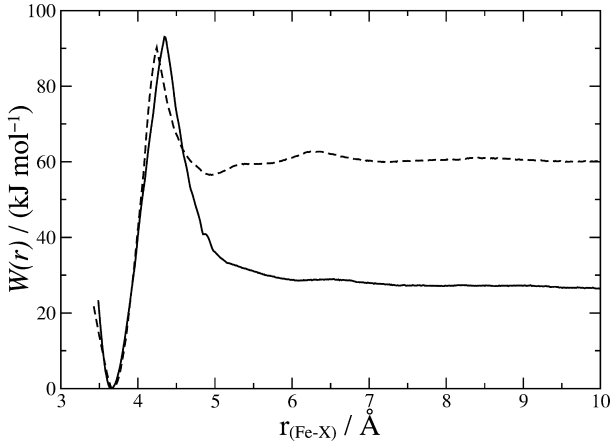

Figure 9. PMFs for XO_4^{n-} exchange with Cl^-, where X = Tc (solid line) and X = S (dashed).

dx.doi.org/10.1021/ct500198c | J. Chem. Theory Comput. 2014, 10, 3345−3353

SO_4^{2-}, respectively, corresponding to exchange rates of 12.6 and 3.0×10^7 s^{-1} at 298 K. No such energy input was required in the case of SO_4^{2-} exchanging with H_2O. The large barriers are due to the electrostatic repulsion between anionic ligands that are forced into close contact during exchange. No energy minima were observed at the point of exchange, suggesting that displacement of Cl^- with an oxyanion also proceeds via an interchange mechanism. TcO_4^- exchange is accompanied by a greater $\Delta H_{ex,aq}$ contribution (−74.5 kJ mol^{-1}) than for SO_4^{2-} (−54.6 kJ mol^{-1}), indicating that the difference between the $T\Delta S_{ex,aq}$ terms (−48.4 kJ mol^{-1} vs 5.4 kJ mol^{-1} for TcO_4^- and SO_4^{2-}, respectively) is enough to overcome the difference in $\Delta H_{ex,aq}$ and is, again, an important factor in determining the selectivity for oxyanions. We find consistency in the difference in $T\Delta S_{ex,aq}$ between the two oxyanions exchanging with H_2O (−54.2 kJ mol^{-1}) and the difference in $T\Delta S_{ex,aq}$ between the corresponding Cl^- exchange events (−53.5 kJ mol^{-1}). Shallow free energy minima, corresponding to hydrogen bonding between the oxyanion and the amine hydrogen atoms, were observed during SO_4^{2-} exchange, most notably at 4.9 Å. There is some evidence that similar energy minima are observed in the equivalent PMF profile for H_2O exchange. On the corresponding *cis* isomers, $\Delta H_{ex,aq}$ was −86.0 and −40.3 kJ mol^{-1} for TcO_4^- and SO_4^{2-} exchange with Cl^-, respectively, increasing the complex's preference for TcO_4^- over SO_4^{2-} relative to the *trans* isomer.

PMF for Direct Exchange of TcO_4^- with SO_4^{2-} on Fe^{3+}−EDA. The Fe^{3+}−EDA complex is initially likely to become saturated with SO_4^{2-}, due to its higher concentration in environmental waters. $\Delta G_{ex,aq}$ for TcO_4^- exchange with SO_4^{2-} is favored by just −4.6 kJ mol^{-1}, in excellent agreement with the difference in $\Delta G_{ex,aq}$ for the two H_2O exchange processes. The PMF profile in Figure 10 reveals that a 97.0 kJ mol^{-1} barrier separates the two configurations. Such a barrier is not insurmountable and is equivalent to an oxyanion exchange rate of 0.22 h^{-1} at 298 K. The atomic coordinates shown in Figure 11 correspond to the positions labeled on the PMF profile in Figure 10. At a Fe^{3+}−Tc distance of 6.5 Å, TcO_4^- approaches the complex in the equatorial plane, minimizing electrostatic repulsion from the SO_4^{2-} ligands. At 4.3 Å, the energy increases significantly as TcO_4^- is forced alongside SO_4^{2-}. After exchange has taken place, the TcO_4^- occupies the axial position and SO_4^{2-} is now forced in the equatorial plane, able to interact with the positively charged amine hydrogen atoms. Notably, the SO_4^{2-} ligand prefers to remain next to the Fe^{3+}−EDA complex after being displaced by TcO_4^-, forming hydrogen bonds with the EDA amine groups, and does not return to solution. The fact that SO_4^{2-} does not fully resolvate in these simulations accounts for an apparent discrepancy between the difference in $T\Delta S_{solv}$ terms for the H_2O ligand exchanges (−54.2 kJ mol^{-1}) and $T\Delta S_{solv}$ for direct exchange of TcO_4^- with SO_4^{2-} (−32.3 kJ mol^{-1}). $\Delta H_{ex,aq}$ for exchange on the *trans* complex is −32.3 kJ mol^{-1}, whereas, for *cis* exchange, the increased electrostatic repulsion from two adjacent SO_4^{2-} destabilizes the initial complex relative to the TcO_4^- coordinated complex and increases the magnitude of $\Delta H_{ex,aq}$ to −59.1 kJ mol^{-1}.

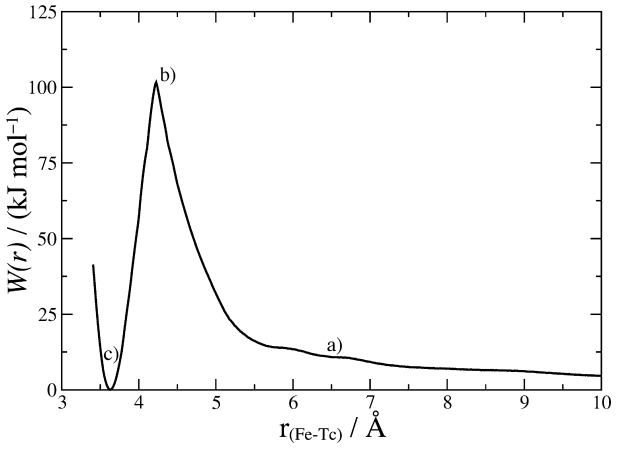

Figure 10. PMF for the exchange of TcO_4^- with SO_4^{2-} on Fe^{3+}−EDA.

Assuming the overall entropy change is the same for ligand exchange on each *cis* complex, as for the *trans* isomer, $\Delta G_{ex,aq}$ can be estimated simply by adding the difference between $\Delta H_{ex,aq}$ for the two isomers to $\Delta G_{ex,aq}$ for the *trans* exchange. Overall, these geometric effects only have a minor effect on $\Delta G_{ex,aq}$, although the results suggest possible enhancement of the selectivity of the sorbent material for TcO_4^- if the Fe^{3+}−EDA monolayer could be tailored so that oxyanion coordination sites were *cis* to each other. The computed $\Delta G_{ex,aq}$ values for exchange at the aqueous Fe^{3+}−EDA complex suggest that TcO_4^- is marginally preferred to SO_4^{2-} unless exchanging with Cl^- anions where the selectivity is switched. Any possible remediation method must be highly selective for TcO_4^- in order to clean up trace quantities. If the performance of an oxyanion-SAMMS material is determined solely by the chemistry of the Fe^{3+}−EDA monolayer complex, it is difficult to see how the experimentally observed distribution coefficients are obtained. Other effects, such as confining the solution to a pore or tethering the complex to the surface, must be, in part, responsible for this selectivity. Our preliminary results for a surface tethered Fe^{3+}−EDA complex suggest that the effect of the amorphous silica substrate may be of importance.

CONCLUSIONS

DFT geometry optimizations were used to guide the parametrization of a classical force field to describe the interactions of oxyanions with a Fe^{3+}−EDA complex. The *trans* isomer of the initial $[Fe(EDA)_2(Cl)_2]^{3+}$ complex was found to be more stable than *cis* by 19.6 kJ mol^{-1}. MD simulations and the umbrella sampling technique were used to generate PMFs to investigate the selectivity of the complex for TcO_4^- and SO_4^{2-}. For an initial Fe^{3+}−EDA complex coordinated by two H_2O ligands, exchange of one H_2O with an oxyanion was found to proceed via an interchange mechanism and the complex preferred to bind TcO_4^- instead of SO_4^{2-}. This preference was replicated in the PMF profile for direct exchange of SO_4^{2-} with TcO_4^-. The free energies associated with these two exchange processes are consistent with each other, but the preference for TcO_4^- is only marginal (approximately 5 kJ mol^{-1}). When Cl^- is coordinated to the initial complex instead, exchange by SO_4^{2-} was preferred. The various contributions to the free energies for aqueous ligand exchange were determined, and the oxyanion solvation entropy was found to be critically important. A better understanding of the use of oxyanion-SAMMS as a TcO_4^- remediation tool could be gained by instead using a full pore model that accounts for the effects of tethering the Fe^{3+}−EDA complex to the surface within a pore of MCM-41.

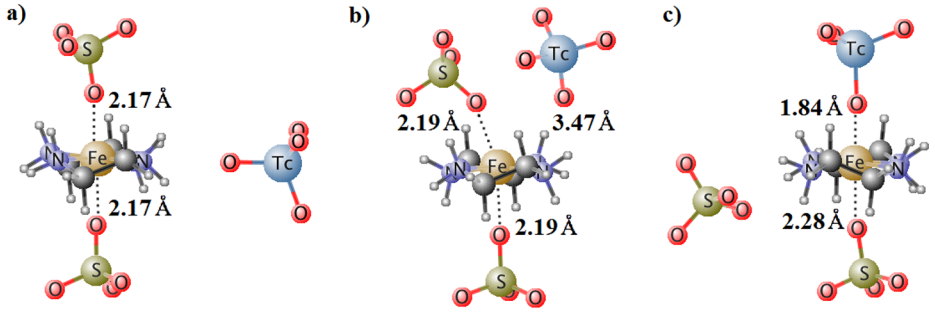

Figure 11. Snapshots obtained from the MD simulations for the exchange of SO_4^{2-} with TcO_4^- from the (a) 6.5, (b) 4.3, and (c) 3.6 Å windows.

■ ASSOCIATED CONTENT

Supporting Information

The Supporting Information contains the full set of classical force field parameters used in this work. This material is available free of charge via the Internet at http://pubs.acs.org.

■ AUTHOR INFORMATION

Corresponding Author

*E-mail: neil.burton@manchester.ac.uk.

Funding

We thank the EPSRC and the Nuclear FiRST Centre for Doctoral Training (CDT) for funding this research. We also acknowledge the use of the University of Manchester Computational Shared Facility.

Notes

The authors declare no competing financial interest.

■ REFERENCES

(1) Schulte, E. H.; Scoppa, P. *Sci. Total Environ.* **1987**, *64*, 163−179.
(2) Watson, J. H. P.; Ellwood, D. C. *Nucl. Eng. Des.* **2003**, *226*, 375−385.
(3) Smith, V.; Fegan, M.; Pollard, D.; Long, S.; Hayden, E.; Ryan, T. P. *J. Environ. Radioact.* **2001**, *56*, 269−284.
(4) Zhang, F.; Parker, J. C.; Brooks, S. C.; Watson, D. B.; Jardine, P. M.; Gu, B. H. *J. Hazard. Mater.* **2010**, *178*, 42−48.
(5) Feng, X.; Fryxell, G. E.; Wang, L. Q.; Kim, A. Y.; Liu, J.; Kemner, K. M. *Science* **1997**, *276*, 923−926.
(6) Kresge, C. T.; Leonowicz, M. E.; Roth, W. J.; Vartuli, J. C.; Beck, J. S. *Nature* **1992**, *359*, 710−712.
(7) Beck, J. S.; Vartuli, J. C.; Roth, W. J.; Leonowicz, M. E.; Kresge, C. T.; Schmitt, K. D.; Chu, C. T. W.; Olson, D. H.; Sheppard, E. W.; McCullen, S. B.; Higgins, J. B.; Schlenker, J. L. *J. Am. Chem. Soc.* **1992**, *114*, 10834−10843.
(8) Fryxell, G. E.; Liu, J.; Mattigod, S. *Mater. Technol.* **1999**, *14*, 188−191.
(9) Fryxell, G. E.; Liu, J.; Hauser, T. A.; Nie, Z. M.; Ferris, K. F.; Mattigod, S.; Gong, M. L.; Hallen, R. T. *Chem. Mater.* **1999**, *11*, 2148−2154.
(10) Kelly, S. D.; Kemmer, K. M.; Fryxell, G. E.; Liu, J.; Mattigod, S. V.; Ferris, K. F. *J. Phys. Chem. B* **2001**, *105*, 6337−6346.
(11) Mattigod, S. V.; Fryxell, G. E.; Parker, K. E. *Inorg. Chem. Commun.* **2007**, *10*, 646−648.
(12) Chouyyok, W.; Wiacek, R. J.; Pattamakomsan, K.; Sangvanich, T.; Grudzien, R. M.; Fryxell, G. E.; Yantasee, W. *Environ. Sci. Technol.* **2010**, *44*, 3073−3078.
(13) Yoshitake, H.; Yokoi, T.; Tatsumi, T. *Chem. Mater.* **2003**, *15*, 1713−1721.
(14) Mattigod, S. V.; Fryxell, G. E.; Alford, K.; Gilmore, T.; Parker, K.; Serne, J.; Engelhard, M. *Environ. Sci. Technol.* **2005**, *39*, 7306−7310.
(15) Zhao, Y.; Truhlar, D. G. *Theor. Chem. Acc.* **2008**, *120*, 215−241.
(16) Andrae, D.; Haussermann, U.; Dolg, M.; Stoll, H.; Preuss, H. *Theor. Chim. Acta* **1990**, *77*, 123−141.
(17) Weigend, F.; Ahlrichs, R. *Phys. Chem. Chem. Phys.* **2005**, *7*, 3297−3305.
(18) Frisch, M. J.; Trucks, G. W.; Schlegel, H. B.; Scuseria, G. E.; Robb, M. A.; Cheeseman, J. R.; Scalmani, G.; Barone, V.; Mennucci, B.; Petersson, G. A.; Nakatsuji, H.; Caricato, M.; Li, X.; Hratchian, H. P.; Izmaylov, A. F.; Bloino, J.; Zheng, G.; Sonnenberg, J. L.; Hada, M.; Ehara, M.; Toyota, K.; Fukuda, R.; Hasegawa, J.; Ishida, M.; Nakajima, T.; Honda, Y.; Kitao, O.; Nakai, H.; Vreven, T.; Montgomery, J. A., Jr.; Peralta, J. E.; Ogliaro, F.; Bearpark, M.; Heyd, J. J.; Brothers, E.; Kudin, K. N.; Staroverov, V. N.; Kobayashi, R.; Normand, J.; Raghavachari, K.; Rendell, A.; Burant, J. C.; Iyengar, S. S.; Tomasi, J.; Cossi, M.; Rega, N.; Millam, J. M.; Klene, M.; Knox, J. E.; Cross, J. B.; Bakken, V.; Adamo, C.; Jaramillo, J.; Gomperts, R.; Stratmann, R. E.; Yazyev, O.; Austin, A. J.; Cammi, R.; Pomelli, C.; Ochterski, J. W.; Martin, R. L.; Morokuma, K.; Zakrzewski, V. G.; Voth, G. A.; Salvador, P.; Dannenberg, J. J.; Dapprich, S.; Daniels, A. D.; Farkas, Ö.; Foresman, J. B.; Ortiz, J. V.; Cioslowski, J.; Fox, D. J. *Gaussian 09*, Revision D.01; Gaussian Inc.: Wallingford, CT, 2009.
(19) Allen, M. P.; Tildesley, D. J. *Computer Simulation of Liquids*; Clarendon Press: Oxford, U.K., 1989.
(20) Huige, C. J. M.; Altona, C. *J. Comput. Chem.* **1995**, *16*, 56−79.
(21) Singh, U. C.; Kollman, P. A. *J. Comput. Chem.* **1984**, *5*, 129−145.
(22) Besler, B. H.; Merz, K. M.; Kollman, P. A. *J. Comput. Chem.* **1990**, *11*, 431−439.
(23) Jorgensen, W. L.; Tiradorives, J. *J. Am. Chem. Soc.* **1988**, *110*, 1657−1666.
(24) Cundari, T. R.; Fu, W. T. *Inorg. Chim. Acta* **2000**, *300*, 113−124.
(25) Ryckaert, J. P.; Ciccotti, G.; Berendsen, H. J. C. *J. Comput. Phys.* **1977**, *23*, 327−341.
(26) Cornell, W. D.; Cieplak, P.; Bayly, C. I.; Gould, I. R.; Merz, K. M.; Ferguson, D. M.; Spellmeyer, D. C.; Fox, T.; Caldwell, J. W.; Kollman, P. A. *J. Am. Chem. Soc.* **1996**, *118*, 2309−2309.
(27) Rizzo, R. C.; Jorgensen, W. L. *J. Am. Chem. Soc.* **1999**, *121*, 4827−4836.
(28) Jorgensen, W. L.; Chandrasekhar, J.; Madura, J. D.; Impey, R. W.; Klein, M. L. *J. Chem. Phys.* **1983**, *79*, 926−935.
(29) Joung, I. S.; Cheatham, T. E., III *J. Phys. Chem. B* **2008**, *112*, 9020−9041.
(30) Smith, W.; Forester, T. R. *J. Mol. Graphics* **1996**, *14*, 136−141.
(31) Hoover, W. G. *Phys. Rev. A* **1985**, *31*, 1695−1697.
(32) Melchionna, S.; Ciccotti, G.; Holian, B. L. *Mol. Phys.* **1993**, *78*, 533−544.
(33) Torrie, G. M.; Valleau, J. P. *J. Comput. Phys.* **1977**, *23*, 187−199.
(34) Bonomi, M.; Branduardi, D.; Bussi, G.; Camilloni, C.; Provasi, D.; Raiteri, P.; Donadio, D.; Marinelli, F.; Pietrucci, F.; Broglia, R. A.; Parrinello, M. *Comput. Phys. Commun.* **2009**, *180*, 1961−1972.
(35) Kumar, S.; Bouzida, D.; Swendsen, R. H.; Kollman, P. A.; Rosenberg, J. M. *J. Comput. Chem.* **1992**, *13*, 1011−1021.
(36) Krebs, B.; Hasse, K. D. *Acta Crystallogr., Sect. B: Struct. Sci.* **1976**, *32*, 1334−1337.
(37) Gancheff, J.; Kremer, C.; Kremer, E.; Ventura, O. N. *J. Mol. Struct.: THEOCHEM* **2002**, *580*, 107−116.

(38) Hay, P. J.; Wadt, W. R. *J. Chem. Phys.* **1985**, *82*, 299−310.
(39) Cannon, W. R.; Pettitt, B. M.; McCammon, J. A. *J. Phys. Chem.* **1994**, *98*, 6225−6230.
(40) Helm, L.; Merbach, A. E. *Chem. Rev.* **2005**, *105*, 1923−1959.